Investigation of the Effect of Tungsten Substitution on Microstructure and Abrasive Wear Performance of *In Situ* VC-Reinforced High-Manganese Austenitic Steel Matrix Composite

EMAD GALIN MOGHADDAM, NEDA KARIMZADEH, NASER VARAHRAM, and PARVIZ DAVAMI

Particulate VC-reinforced high-manganese austenitic steel matrix composites with different vanadium and tungsten contents were synthesized by conventional alloying and casting route. Microstructural characterizations showed that the composites processed by *in situ* precipitation of the reinforcements were composed of V_8C_7 particulates distributed in an austenitic matrix. It was observed that addition of tungsten to austenite increases work-hardening rate of subsurface layer during pin-on disk wear test. The maximum abrasive wear resistance was achieved at tungsten content equal to 2 wt pct. However, excessive addition of tungsten promoted the formation of W_3C phase and reduced the abrasive wear resistance because of decrease in distribution homogeneity and volume fraction of the reinforcing VC particles.

DOI: 10.1007/s11661-013-1733-8

I. INTRODUCTION

WITH the development of industrial processes demanding more resistant materials in terms of corrosion, oxidation, and mechanical properties, establishing economic production techniques of new materials with enhanced characteristics is crucial. For example, *in situ* production of iron matrix composites has received much interest worldwide during the last three decades due to the following reasons:

(1) The process enables the formation of clean interfaces, *i.e.*, free from adsorbed gases, oxides, or other detrimental surface reactions. This in turn tends to make the matrix–filler interface bond strong.
(2) The process of generation of the filler phase *in situ* excludes the manufacture and the handling of the phase separately, thereby reducing the unit steps in the process.
(3) Near-net shape final components can be produced by direct casting.[1]

Therefore, this synthesis method provides a scope of producing relatively inexpensive wear-resistant composite materials *via* formation of hard intermetallic particle reinforcements within the solidifying steel matrix in contrast to the powder metallurgy technique.[2–6]

The most common ceramic materials used for reinforcing of various types of steel matrices are Al_2O_3, ZrO_2, Si_3N_4, Cr_3C_2, TiN, TiB_2, TiC, B_4C, WC, VC, *etc.*[3,7] Among them vanadium carbide (VC) has proved to be a unique choice to increase the wear resistance of martensitic steel matrices[8–13] due to its superior hardness of about 2600 to 3000 HV.[14] On the other hand, it is well known that austenite possesses higher toughness in comparison with the martensite. Therefore, from the fracture-failure point of view, a composite with austenitic matrix comprises less potential risk for engineering application than a martensitic one. Recently, *in situ* VC-reinforced high-manganese austenitic steel matrix composite has been produced, offering a combination of good impact toughness and excellent abrasive wear resistance. It was observed that the austenitic steel with 3 pct carbon and 10 pct vanadium exhibited the highest mechanical and wear properties.[15]

Similar to vanadium, tungsten is also a strong carbide-forming element.[16,17] Its maximum solubility in austenite is about three times of that of the vanadium[18] and is expected to strengthen the vulnerable austenite matrix against the abrasive particles by solution hardening and formation of very hard carbides.[19] Therefore, the current study highlights the effect of substitution of vanadium with tungsten on microstructure and abrasive wear performance of *in situ* VC-reinforced austenitic steel–matrix composite material.

II. EXPERIMENTAL PROCEDURES

A. *Materials and Synthesis*

The synthesis of the composites was carried out using a basic lining, medium-frequency induction furnace. High manganese steel ingots were initially heated up to

EMAD GALIN MOGHADDAM, Senior Researcher, NASER VARAHRAM, Associate Professor, and PARVIZ DAVAMI, Professor, are with the Department of Materials Science and Engineering, Sharif University of Technology, Tehran, Iran. Contact e-mails: emad_g_moghaddam@alum.sharif.edu, emad.g.moghaddam@gmail.com NEDA KARIMZADEH, Senior Researcher, is with the Department of Materials Engineering, Islamic Azad University, Najafabad Branch, Isfahan, Iran.

Manuscript submitted August 23, 2012.
Article published online April 12, 2013

Table I. Chemical Composition of the Casting Composites (Weight Percentage)

Alloy	C	Mn	Cr	V	W	V + W	Fe
10V0W	3.03	13.08	0.32	10.14	0.03	10.17	base
9V1W	3.04	12.93	0.34	9.17	0.98	10.15	base
8V2W	3.02	13.11	0.31	8.02	2.02	10.04	base
7V3W	3.05	13.14	0.28	7.06	3.08	10.14	base
6V4W	2.99	13.17	0.29	6.03	4.06	10.09	base
5V5W	3.01	13.07	0.29	5.01	5.12	10.13	base

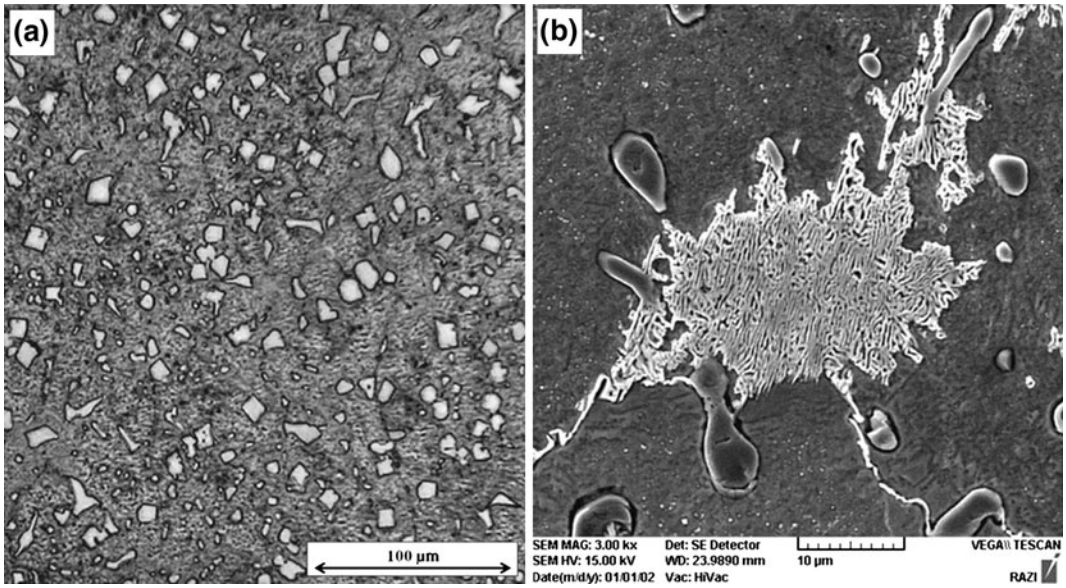

Fig. 1—(*a*) Microstructure of the as-cast 10V0W alloy and (*b*) lamellar $(Fe,Mn)_3C$ eutectic phase in VC-reinforced high-manganese austenitic steel matrix composites.

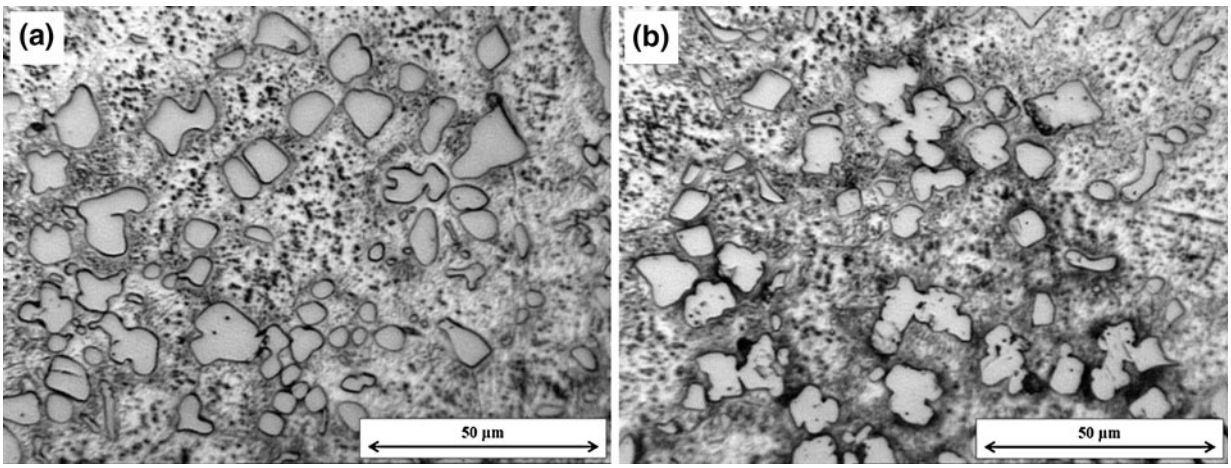

Fig. 2—(*a*) Microstructure of the as-cast 9V1W alloy and (*b*) microstructure of the as-cast 8V2W alloy.

1773 K (1500 °C) and maintained at this temperature for 10 minutes. Then, the temperature was raised to 1823 K (1550 °C) and calculated amounts of vanadium and tungsten were added to the melts in form of low-carbon ferroalloys, respectively. The interval between the addition of vanadium and tungsten was 5 minutes. After 10 minutes, the temperature was lowered to 1773 K (1500 °C), and the final composition of the melts was adjusted by adding the required amounts of manganese and carbon. Finally, the melts were

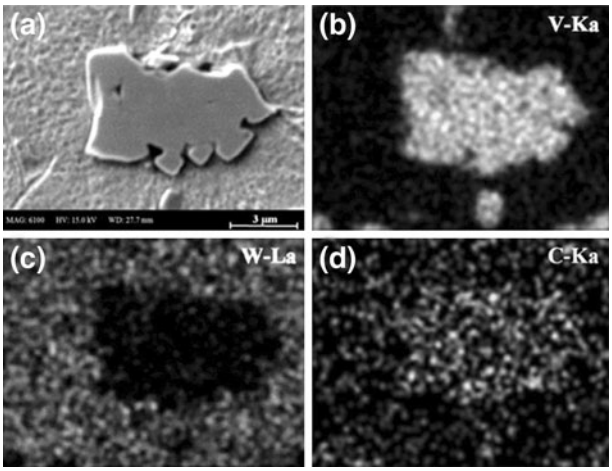

Fig. 3—EDS analysis of the as-cast 8V2W alloy: (*a*) SEM image, (*b*), (*c*), and (*d*) are the elemental maps of V, W, and C, respectively.

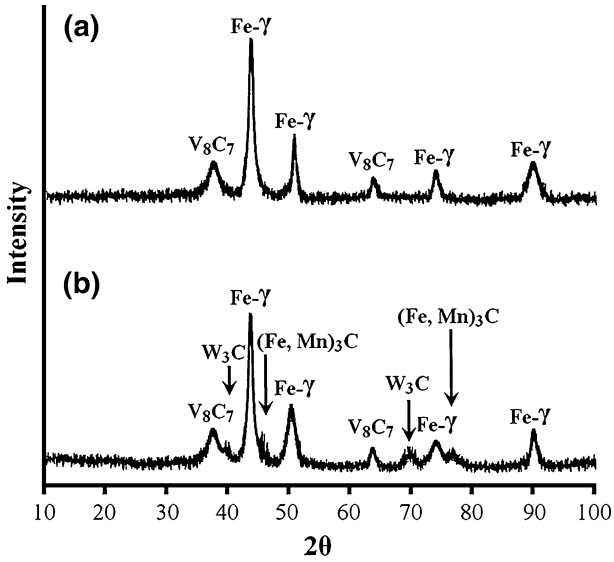

Fig. 4—X-ray diffraction patterns of the materials in as-cast condition: (*a*) 8V2W and (*b*) 6V4W composites.

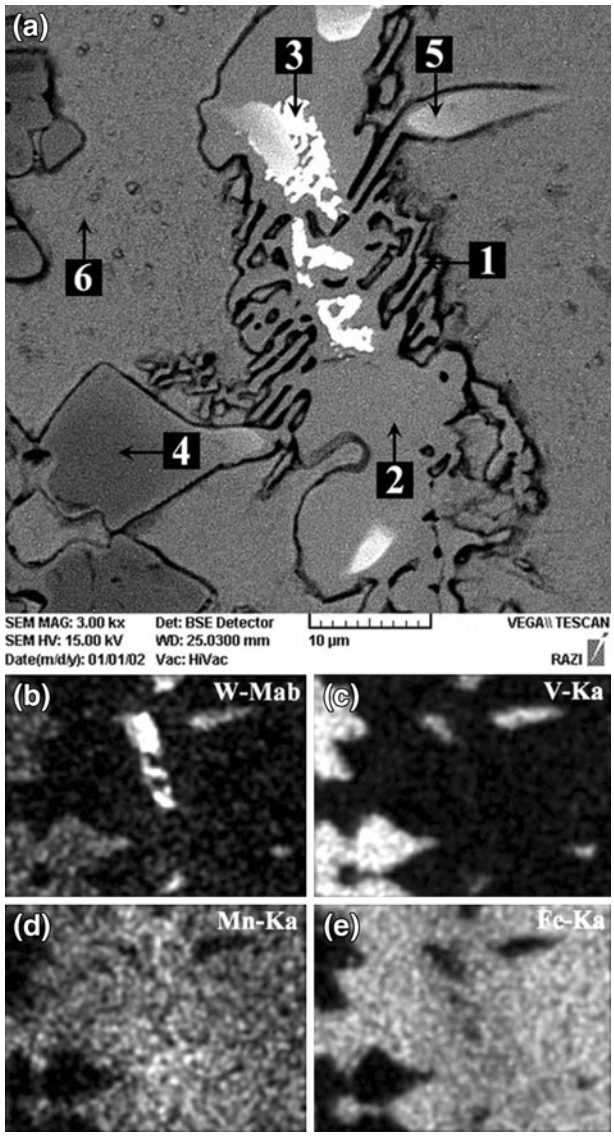

Fig. 5—(*a*) Back-scattered electron image of grain boundary complex carbide in as-cast 7V3W alloy, (*b*), (*c*), (*d*), and (*e*) are EDS elemental maps of W, V, Mn, and Fe of the corresponding images, respectively.

deoxidized with 0.1 wt pct pure aluminum and poured in preheated investment ceramic molds at 1753 K to 1793 K (1480 °C to 1520 °C).

Some of the casting composites from each alloy composition (shown in Table I) were subjected to solution treatment at 1373 K (1100 °C) for 90 minutes and then water quenched. While heating, to prevent surface decarburization, the samples were covered by cast iron chips in a sealed box.

B. *Materials Characterization*

Metallographic specimens were prepared according to conventional laboratory techniques and etched with 5 pct Nital (5 mL HNO_3 + 95 mL ethanol) followed by immersion in 15 pct HCL solution to remove staining. The density of the materials was determined by the Archimedes' method in distilled water, using an analytic balance equipped with a density measurement kit. Microstructure of the materials was studied by optical and scanning electron microscopes (Olympus BX51 M and TESCAN VEGAII XMU, respectively). XRD analysis was performed with Cu-K_α radiation to identify the phase type using a Philips Xpert diffractometer. Microhardness measurements of the matrices were carried out using LEITZ WETZLAR microhardness tester under loading of 300 g (HV0.3) for 15 seconds. Samples for Charpy unnotched impact test were also prepared as per ASTM E-23.[20]

Dry sliding wear resistance of the materials was evaluated with pin-on-disk test method. Samples were prepared as pins with a cross section of 10 × 10 mm^2. For each sample, the abrasion test was run under a load of 75 Newton on a fresh 120 grit SiC abrasive paper affixed to a rotating disk. The rotation speed of the disk

Table II. EDS Microanalysis of Regions in Fig. 5(a) (Weight Percentage)

Probe Points	C	Mn	Cr	V	W
Point 1	3.79	18.27	0.47	1.45	4.62
Point 2	1.97	20.89	1.02	3.61	5.63
Point 3	7.77	3.07	0.97	13.22	67.39
Point 4	6.04	2.11	1.07	72.20	10.04
Point 5	7.52	1.38	0.75	40.82	45.63
Point 6	2.40	11.69	0.09	1.22	2.49

The presented values are only for comparison and might be associated with some errors especially for carbon element.

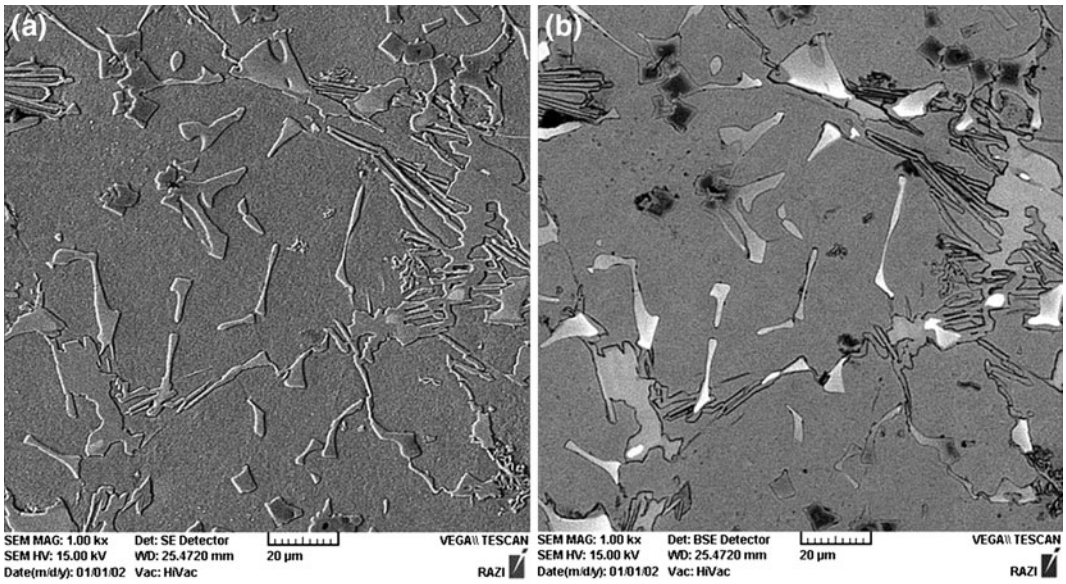

Fig. 6—Distribution of tungsten through the microstructure of a high-vanadium high-tungsten austenitic manganese steel, the 6V4W alloy: SEM (*a*) secondary electron and (*b*) back-scattered electron image.

was fixed at 60 rpm. The specimen holder was designed in a manner to move the samples backward and forward on the abrasive paper at a constant speed of 10 mm/s, making a helical track of approximately 1.5 m in length, repeatedly. This procedure assured that, the specimen always encountered fresh abrasive particles. The total length of wear path for each sample was 600 m, with a pause after every 30 m for weighting it. At every pause, the samples were cleaned with ethanol and weighed. The weight loss was converted to volume loss, and then wear data were plotted as cumulative volume loss, as a function of sliding distance. The wear rate of each specimen was calculated using Eq. [1]:

$$\text{Wear rate } (\text{mm}^3/\text{m}) = \frac{\text{Mass loss (g)}/\text{Density (g/mm}^3)}{\text{Sliding distance (m)}}. \quad [1]$$

III. RESULTS AND DISCUSSION

A. *Microstructural Study*

The presence of large amounts of vanadium in the chemical composition of the melts promotes the formation of very hard carbides in the microstructure. The mechanism of the formation of VC particles can be described as follows. Solidification initiates through nucleation and growth of vanadium carbide particulates in molten steel. This leads to plentiful precipitation of coarse primary VC particles in the structure. When tungsten is presented in alloy composition, its solubility decreases as the temperature of the molten alloy is further reduced, and an over-saturated solution of tungsten is formed around solid particles. Hence, tungsten comes out from the melt and enters into the growing VC particles. Solidification proceeds with the crystallization of the iron matrix around the particulates and ends with formation of eutectic $(Fe,Mn)_3C$ phase at grain boundaries. Manganese contributes a vital austenite-stabilizing effect, operating to delay transformation rather than to eliminate it,[21] wherein in a steel containing 13 wt pct Mn, the metallic matrix at ambient temperature is expected to be fully austenitic. Microstructure of the as-cast VC-reinforced high-manganese austenitic steel matrix composite (10V0W) is shown in Figure 1(a). The primary spherical vanadium carbides (V_8C_7 in chemical stoichiometry) are uniformly dispersed inside the austenite grains. Besides, negligible amounts of lamellar $(Fe,Mn)_3C$ eutectic phase are found at triple grain boundary junction (Figure 1(b)).[15]

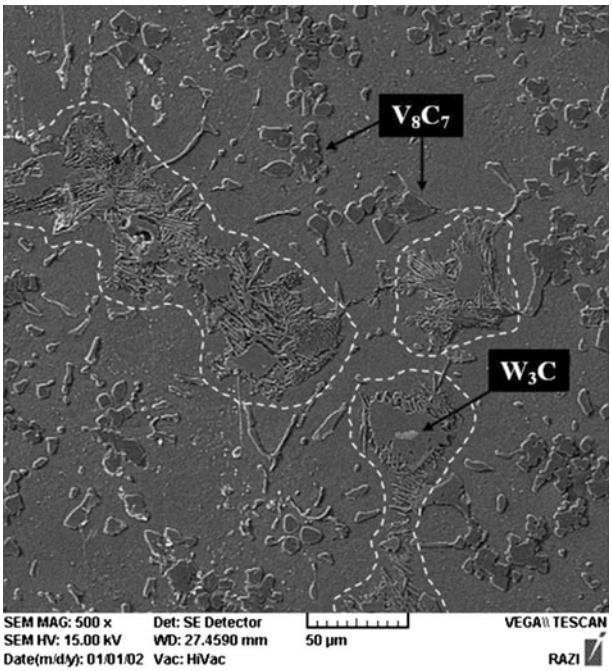

Fig. 7—As-cast microstructure of the 6V4W alloy: dashed lines depict the eutectic $(Fe,Mn)_3C$ phase.

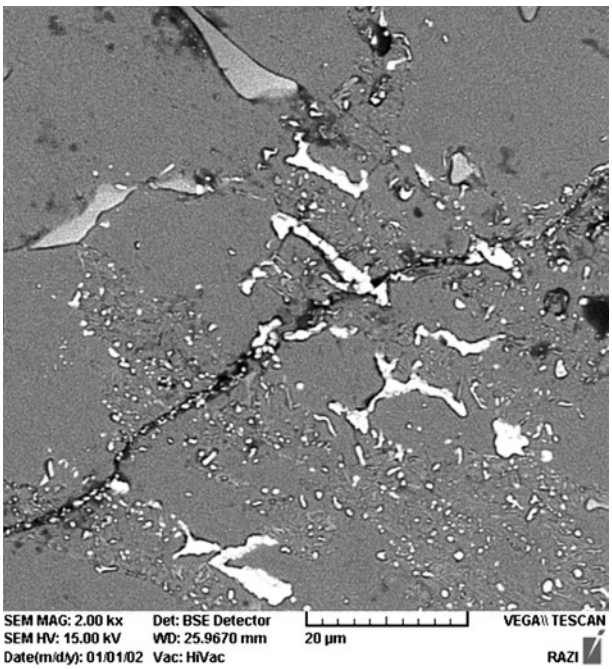

Fig. 8—Typical microstructure of austenite grain boundary in the studied high-tungsten composites after the solutionizing heat treatment.

Substitution of vanadium with 1 to 2 wt pct tungsten in 9V1W and 8V2W composites caused only slight variations in shape regularity of primary vanadium carbides (Figure 2), as most of the tungsten tended to dissolve in the austenite rather than VC lattice, because the solubility limit of tungsten in austenite is roughly three times of that of vanadium. Figure 3 shows an

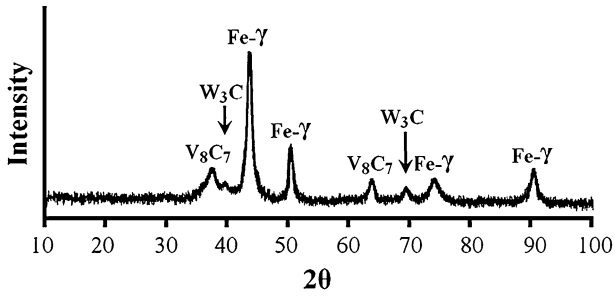

Fig. 9—X-ray diffraction patterns of 6V4W composite in the heat-treated condition.

example of EDS analysis of the microstructure of 8V2W composite, where (a) is SEM image, and (b), (c), and (d) are the elemental maps of V, W, and C, respectively. It is clear that the matrix contains higher concentration of tungsten relative to primary vanadium carbide. Moreover, no indication of tungsten carbide or the $(Fe,Mn)_3C$ phase was observed in the X-ray analysis diffraction patterns of the two above composites (Figure 4(a)).

Upon further increasing the tungsten and decreasing the vanadium contents, microstructure of the composites changed significantly and coarse irregular-shaped phases appeared in the matrix, mostly at grain boundary junctions, which were composed of three distinct regions. These areas are shown in Figure 5(a)—regions 1, 2, and 3, respectively, as Lamellar or acicular iron-manganese carbide growing into the adjacent austenite grain (the outer region), monolithic iron-manganese carbide (the middle region), and the interior region which was the tungsten carbide. XRD analysis proved that it is of the type W_3C (Figure 4(b)). This carbide is capable of dissolving a certain quantity of vanadium clarified by EDS microanalysis (Table II). On the contrary, in 7V3W, 6V4W, and 5V5W composites, primary vanadium carbides contained higher concentration of tungsten in chemical composition relative to the austenite, and their morphology changed from spherical or bulky to chicken-feet-like shape. Moreover, tungsten atoms were not evenly distributed within the vanadium carbides. For illustration, SEM secondary and back-scattered electron images of the 6V4W composite are presented in Figure 6. The brighter regions in Figure 6(b) indicate higher concentration of tungsten. It is noteworthy that substitution of vanadium with tungsten increased the total amount of $(Fe,Mn)_3C$ eutectic phase in the materials. In steels, the major carbide-forming elements in the order of increasing the affinity for carbon are Mn, Cr, W, Mo, V, Ti, Zr, Ta, and Nb.[22] Therefore, bearing in mind that the total amount of vanadium and tungsten were kept constant (Table I: wt pct V + wt pct W $\approx$ 10) and the fact that vanadium is a stronger carbide-forming element than tungsten, it is understood that with substitution of V with W, more carbon is available to react with weaker carbide-forming elements such as iron and manganese. Typical microstructure of the as-cast high-tungsten composites in the current study is shown in Figure 7,

Table III. Microhardness, Volume Fraction of Reinforcements, and Impact Toughness of the Investigated Casting Composites

Casting Composites	Matrix Microhardness (HV0.3) Error = 1.51 pct		Volume Fraction of Reinforcements Error = 2.67 pct		Impact Toughness (J) Error = 2.14 pct		TI* (pct)
	As-Cast	Heat-Treated	V_8C_7	W_3C	As-Cast	Heat-Treated	
10V0W	585	560	20.07	0	32	36	11.1
9W1W	592	566	19.26	0	31	35	11.4
8V2W	606	569	18.41	0	27	33	18.2
7V3W	611	571	15.26	2.38	22	28	21.4
6V4W	615	574	13.63	3.49	16	21	23.8
5V5W	620	576	12.02	4.73	12	16	25.0

*Toughness improvement.

where the dashed lines depict the eutectic $(Fe,Mn)_3C$ phase.

Figure 8 is a typical microstructure of austenite grain boundary in the studied VC-reinforced high-tungsten composites (the 7V3W, 6V4W, and 5V5W alloys) after the applied heat treatment. Comparison of the micrograph with Figure 5(a) reveals that solution annealing at 1373 K (1100 °C) for 90 minutes was able to dissolve the iron-manganese carbides in the matrix and subsequent water quench prevented them from precipitating at grain boundaries. Complete dissolution of $(Fe,Mn)_3C$ carbides was supported by the XRD diffraction pattern of the materials after the solutionizing heat treatment (Figure 9). However, it was observed that the above solution treatment could not decompose tungsten carbides back into the austenite matrix. Further microstructural studies showed that only slight changes in VC morphologies was distinguishable compared with the as-cast condition, such as breaking the network carbides at weak connection areas and dissolution of carbides at sharp edges. This could be related to high stability of vanadium and tungsten carbides at elevated temperature as both V and W are known to be strong carbide-forming elements (the affinity for carbon by an element is in conformity with the stability of the carbide of the element). In practice, it is nearly impossible to dissolve these carbides with conventional austenitizing–quenching treatments below 1473 K (1200 °C).[22–26]

B. *Mechanical Properties*

Table III lists Vickers microhardness of the matrix, volume fraction of the reinforcements, and Charpy unnotched impact toughness of the synthesized materials. The microhardness measured values show that as more tungsten is introduced to the chemical compositions, a harder austenitic is achieved compared with the matrix of the 10V0W composite. This is associated with the higher solubility of tungsten in austenite, which provides extra solution hardening of the matrix.

Among the various mechanical characteristics of the metals, impact toughness might be considered to be very dependent on microstructural parameters such as morphology and distribution of the microstructural constituents. Hard, brittle, and elongated phases can significantly deteriorate the impact toughness.[27–31] In the studied composites, as the tungsten content increased, shape regularity of vanadium carbides was decreased. This was followed by increasing the hardness of the matrix, leading to lower impact toughness. Moreover, where the total affinity for carbon was comparatively low (the 7V3W, 6V4W, and 5V5W composites), more eutectic $(Fe,Mn)_3C$ precipitated along the grain boundaries, weakening the bonding between the austenite grains in the as-cast condition. Consequently, when subjected to impact, cracks easily initiate and grow along the boundaries between eutectic carbides and grains due to the higher brittleness of carbide phase in comparison with the austenite and fracture occurs at lower impact energies. Therefore, elimination of these brittle phases improved the impact toughness. This is supported by the impact toughness improvement percentage after the applied solution heat treatment (Table III).

C. *Abrasive Wear Resistance*

Figures 10(a) and (b) show cumulative volume loss and wear rate of the synthesized composites in the heat-treated condition. It has been observed that the cumulative volume loss was approximately linear with the sliding distance, except at the commencement of the abrasion test (Figure 10(a)). It is clear form Figure 10(b) that the wear rates of the materials were higher at the beginning of the test, then decreased with increasing the sliding distance, and then finally leveled off after a certain test period. Therefore, removal of material from the surface can be divided into three stages: initial wear, transient wear, and uniform wear. In the initial wear stage, SiC particles can easily deform and remove the material from soft austenitic matrix and the wear rate is high. This deformation introduces a large strain at the surface of the material which tends to induce dislocations in the subsurface regions of the matrix. Accumulation of dislocations leads to the formation of a work-hardened surface layer on top surface regions resulting in a decrease in wear rate at the transient stage.[32] According to experimental results, the transient wear in

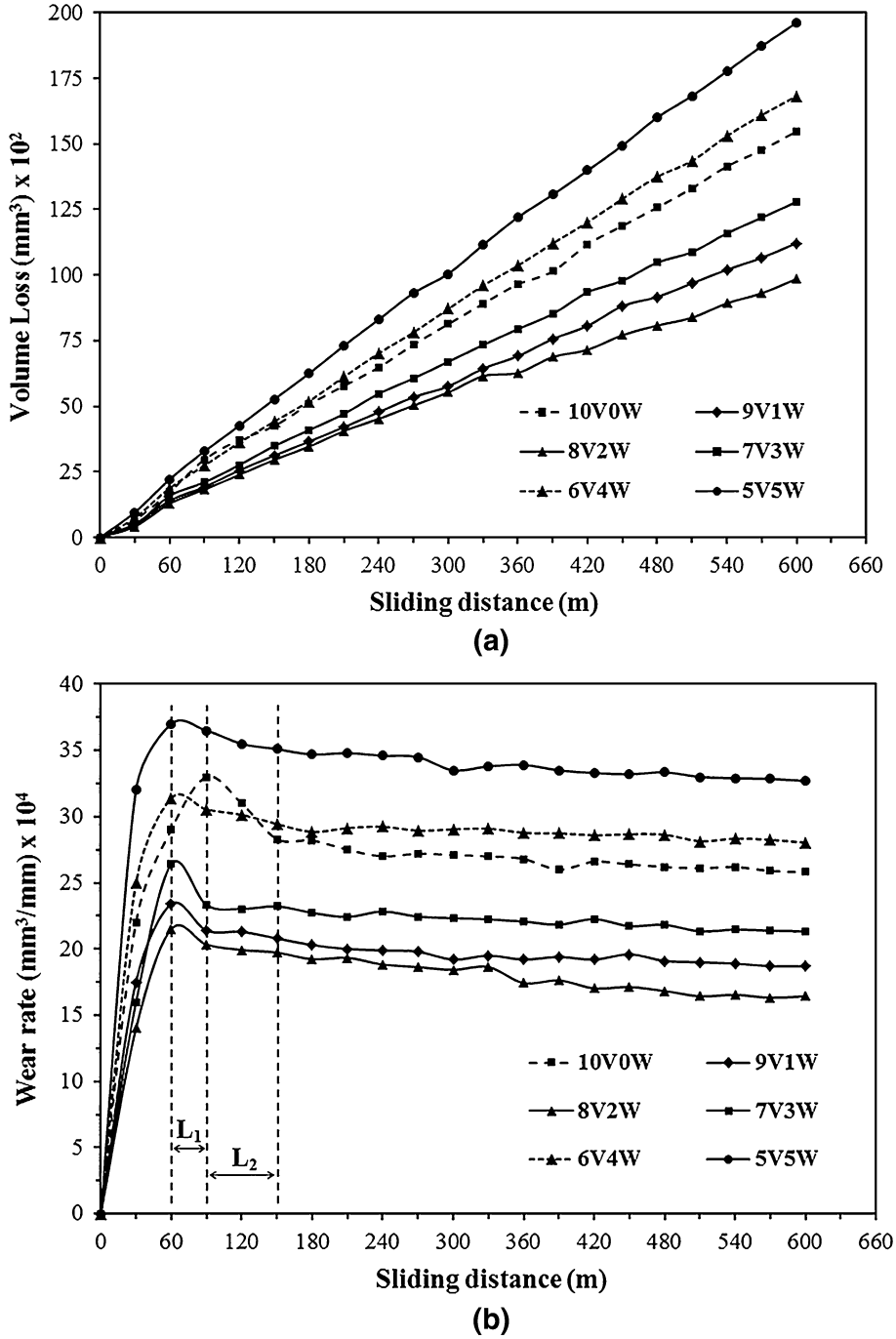

Fig. 10—(*a*) Cumulative volume loss and (*b*) wear rate of the investigated composites. L_1 and L_2 indicate transient wear stage of the W-containing and the 10V0W composites, respectively.

tungsten-containing VC-reinforced composites initiated after 60 m of sliding and lasted up to a sliding distance of 90 m (L_1), while for the 10V0W alloy, it was determined to be from 90 m to 150 m (L_2). This can probably be attributed to the effect of tungsten to increase work-hardening rate of the austenite. The uniform wear stage begins where the rate of material removal from the surface is approximately equal to the work-hardening rate of the matrix. Therefore, with the increasing sliding distance beyond the transient stage, the wear rate of the composites remained constant. Figure 11 illustrates the hardness distribution of the matrix from top worn surface along the cross section of the specimens. As can be seen, the austenite matrix is much harder at the surface layer compared with the inner core of the specimens. This is attributed to the

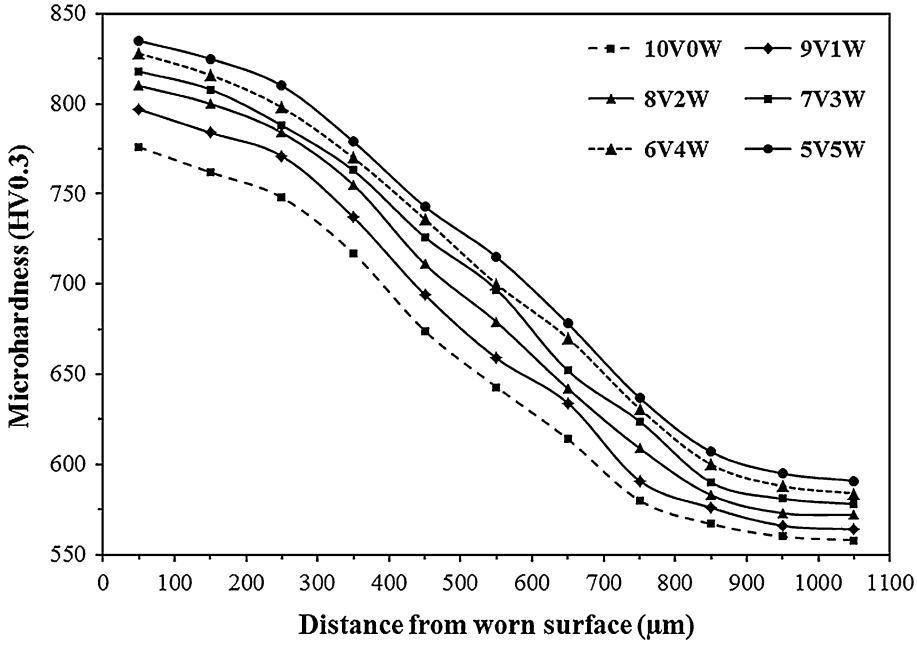

Fig. 11—Hardness distribution of the worn austenite matrix.

high work-hardening capacity of the austenite due to the plastic deformation of surface layers.

Figure 12 illustrates the abrasive wear resistance of the investigated composite materials which is defined as the inverse of magnitude of wear rate at the uniform wear stage of the individual samples. The wear resistance of 10V0W is considered to be equal to unity, and the wear resistance of the others is calculated relative to this composite. In the investigated materials, the *in situ* formed VC particles act as main load-bearing constituents, which retains at the sliding surface of the composite and resist microcutting and plastic deformation of the matrix caused by SiC particles. Therefore, the wear resistance of the studied materials is strongly affected by hardness, volume fraction, and distribution of the reinforcements, as well as the hardness of the surrounding austenite itself. As mentioned above, distribution homogeneity of VC particles was not seriously affected by substituting 1 or 2 wt pct tungsten in chemical composition of 10V0W alloy. However, the hardness of the matrix was increased with the increase of tungsten as shown in Table III. It can be seen that, although the volume fraction of the reinforcements has decreased through substitution of vanadium with tungsten, but the associated wear-resistance enhancement was remarkable from 10V0W to 8V2W composite. The maximum improvement in abrasive wear resistance was nearly 60 pct in the case of 8V2W material which is explained by increasing the initial hardness and work-hardening rate of the austenite that could compensate the negative feature of lower volume fraction of VC particles in 9V1W and 8V2W composite materials compared with 10V0W alloy. However, it was observed that further substitution of vanadium with tungsten was detrimental to the abrasive wear resistance in 7V3W, 6V4W, and 5V5W composites. As mentioned above,

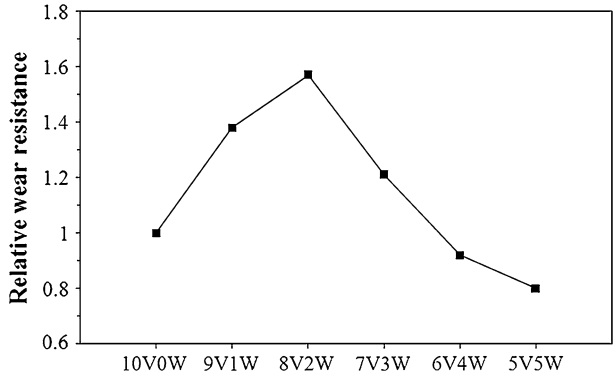

Fig. 12—Relative wear resistance of the investigated materials.

with increasing tungsten content in chemical composition while keeping the total wt pct V + wt pct W constant, shape regularity and dispersion homogeneity of the carbides were decreased leaving much of the matrix surface area unprotected against abrasive particles. In addition, the existing tungsten carbides in these alloys exhibited lower hardness compared with the VC particles (the measured Vickers hardness values were 2310 HV and 2650 HV for W_3C and VC, respectively). It is to be noted that although the value for the hardness of the existing tungsten carbide phase was seemingly rather high, it has been reported that W_3C can be harder than WC carbide,[33,34] having a hardness in the range of 2000 to 2500 HV.[34] In addition, the presence of more than 13 pct vanadium in the structure of W_3C phase in the alloys of the current study might have a positive role to increase its hardness (Table II). However, the two above mentioned parameters were concurrent with reduction of the total amount of reinforcing particles

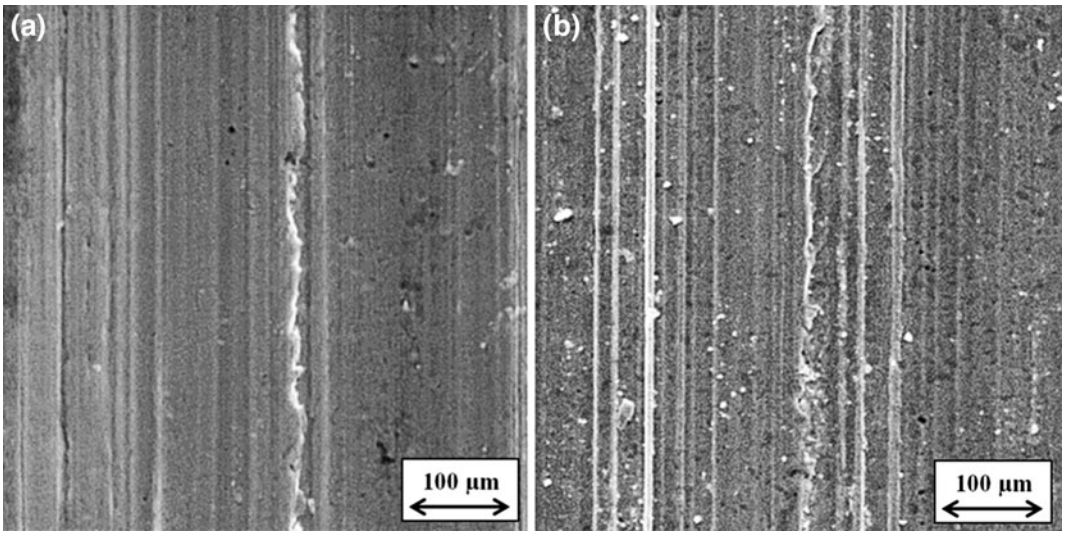

Fig. 13—SEM micrographs of the worn surface of (*a*) 8V2W and (*b*) 5V5W composite.

which could increase the plastic deformation of the worn surface due to microplowing of SiC particles as shown in Figure 13. Consequently, the abrasive wear resistance was decreased as the content of tungsten exceeded 2 wt pct in the studied VC-reinforced composite materials.

IV. CONCLUSIONS

(1) *In-situ* production of VC-reinforced high-manganese steel matrix composite is feasible by conventional melting and casting route. The microstructure of the composite alloys is composed of VC particles precipitated in austenitic matrix when the concentration of tungsten is ≤2 wt pct. Further substitution of vanadium with tungsten promotes the formation of W_3C phase.

(2) Addition of tungsten to austenite increases the initial hardness and work-hardening rate of the matrix. Higher work-hardening rate accelerates the commencement of transient and the subsequent uniform wear stage and decreases the materials loss during abrasion.

(3) Solution annealing at 1373 K (1100 °C) annihilates the detrimental effect of $(Fe,Mn)_3C$ precipitates in VC-reinforced high-manganese austenitic steel matrix composite and improves impact toughness.

(4) With the increase of tungsten, the volume fraction and dispersion homogeneity of vanadium carbides decrease, which leads to the reduction of the abrasive wear resistance of VC-reinforced composite materials when wt pct W exceeds 2 wt pct. Therefore, in the above composite materials, the substitution of vanadium with more than 2 wt pct tungsten is not recommended for engineering applications because of comparatively poor impact toughness and abrasive wear resistance.

ACKNOWLEDGMENTS

The authors wish to acknowledge extensive financial and experimental support of the R&D Division of Tabarestan Steel Foundry Company (TSF) and Razi Metallurgical Research Center (RMRC) for the current study.

REFERENCES

1. K. Das, T.K. Bandyopadhyay, and S. Das: *J. Mater. Sci.*, 2002, vol. 37, pp. 3881–92.
2. W.H. Jiang, W.D. Pan, Y.L. Ren, and X.L. Han: *J. Mater. Sci. Lett.*, 1998, vol. 17, pp. 1527–29.
3. E. Pagounis and V.K. Lindroos: *Mater. Sci. Eng. A*, 1998, vol. 246, pp. 221–34.
4. T.K. Bandyopadhyay, S. Chatterjee, and K. Das: *J. Mater. Sci.*, 2004, vol. 39, pp. 5735–42.
5. T.K. Bandyopadhyay and K. Das: *J. Mater. Sci.*, 2004, vol. 39, pp. 6503–08.
6. K. Das and T.K. Bandyopadhyay: *Mater. Lett.*, 2004, vol. 58, pp. 1877–80.
7. A.K. Srivastava and K. Das: *Mater. Sci. Eng. A*, 2009, vol. 516, pp. 1–6.
8. S. Wei, J. Zhua, and I. Xua: *Tribol. Int.*, 2006, vol. 39, pp. 641–48.
9. S. Wei, J. Zhua, I. Xua, and L. Rui: *Mater. Des.*, 2006, vol. 27, pp. 58–63.
10. K. Tokaji, Y. Uematsu, T. Horie, and Y. Takahashi: *Mater. Sci. Eng. A*, 2006, vol. 418, pp. 326–34.
11. Y. Uematsu, K. Tokaji, T. Horie, and K. Nishigaki: *Mater. Sci. Eng. A*, 2007, vol. 471, pp. 15–21.
12. K. Shimizu, T. Naruse, Y. Xinba, K. Kimura, K. Minami, and H. Matsumoto: *Wear*, 2009, vol. 267, pp. 104–09.
13. Y. Uematsu, K. Tokaji, K. Nishigaki, D. Okajima, and M. Ogasawara: *Mater. Sci. Eng. A*, 2010, vol. 527, pp. 2621–28.
14. L. Xu, S. Wei, J. Xing, Y. Li, and R. Long: *Met. Mater. Int.*, 2006, vol. 12 (5), pp. 371–75.
15. E.G. Moghaddam, N. Varahram, and P. Davami: *Mater. Sci. Eng. A*, 2012, vol. 532, pp. 260–66.
16. S.H. Mousavi Anijdan, A. Bahrami, N. Varahram, and P. Davami: *Mater. Sci. Eng. A*, 2007, vols. 454–455, pp. 623–28.
17. G. Roberts, G. Krauss, and R. Kennedy: *Tool Steels*, 5th ed., ASM International, Materials Park, OH, 1998, p. 283.
18. *ASM Handbook, Vol 3: Alloy Phase Diagrams*, ASM International, Materials Park, OH, 1992.
19. T.S. Eyre: *Tribol. Int.*, 1976, vol. 9 (5), pp. 203–12.

20. ASTM E-23-2a, Standard Test Methods for Notched Bar Impact Testing of Metallic Materials, *Annual Book of ASTM Standards*, vol. 0.3.01, 1998.
21. *ASM Handbook, Vol 1: Properties and Selection: Irons, Steels, and High-Performance Alloys*, ASM International, Materials Park, OH, 2005.
22. J.H. Davidson: *Microstructure of Steels and Cast Irons*, Springer, New York, 2004, p. 264.
23. W.B. MacKay and R.W. Smith: US Patent No. 4377422, 1983.
24. A.G. Rakhshtadt, K.A. Lanskaya, and V.V. Goryachev: *Metallovedenie i Termicheskaya Obrabotka Metallov*, 1981, vol. 2, pp. 21–25.
25. V.M. Kardonskii and O.V. Samoilova: *Metallovedenie i Termicheskaya Obrabotka Metallov*, 1990, vol. 8, pp. 59–61.
26. A.G. Rakhshtadt, K.A. Lanskaya, N.M. Suleimanov, and L.V. Katkova: *Metallovedenie i Termicheskaya Obrabotka Metallov*, 1975, vol. 6, pp. 23–27.
27. A.S. Chaus: *Met. Sci. Heat Treat.*, 1998, vol. 40, pp. 15–20.
28. A.S. Chaus: *Met. Sci. Heat Treat.*, 2003, vol. 45, pp. 3–7.
29. H. Fua, Q. Xiao, and Y. Li: *Mater. Sci. Eng. A*, 2005, vol. 395, pp. 281–87.
30. A.S. Chaus: *Met. Sci. Heat Treat.*, 2005, vol. 47, pp. 16–21.
31. A.S. Chaus: *Phys. Met. Metallogr.*, 2008, vol. 106, pp. 82–89.
32. A.K. Srivastava and K. Das: *Tribol. Int.*, 2010, vol. 43, pp. 944–50.
33. B.G. Mellor: *Surface Coatings for Protection Against Wear*, Woodhead, Cambridge, 2006, p. 132.
34. N.J. Archer and K.K. Yee: *Wear*, 1978, vol. 48, pp. 237–50.